Transition from unidirectional to delayed bidirectional coupling in optically coupled semiconductor lasers

Cristian Bonatto,[1,2] Bryan Kelleher,[1,2] Guillaume Huyet,[1,2] and Stephen P. Hegarty[2]
[1]*Centre for Advanced Photonics and Process Analysis, Cork Institute of Technology, Bishopstown, Cork, Ireland*
[2]*Tyndall National Institute, University College Cork, Lee Maltings, Dyke Parade, Cork, Ireland*
(Received 16 November 2010; revised manuscript received 15 November 2011; published 6 February 2012)

We investigate the transition from unidirectional to delayed bidirectional coupling of semiconductor lasers. By tuning the coupling strength in one direction we show how the locking region evolves as a function of the detuning and coupling strength. We consider two representative values of the relaxation oscillation damping: one where the relaxation oscillations are very underdamped and one where they are very overdamped. Qualitatively different dynamical scenarios are shown to emerge for each case. Several features of the delayed bidirectional system can be seen as remaining from the unidirectional system while others clearly arise due to the delayed coupling and are similar to effects seen in delayed feedback configurations.

DOI: 10.1103/PhysRevE.85.026205 PACS number(s): 05.45.Xt, 42.55.Px, 42.65.Sf

I. INTRODUCTION

The dynamics of interacting oscillators is a subject of considerable interest in many areas of science within physics, chemistry, and biology [1]. Many natural and engineered systems can be described by a number of individual oscillators interacting according to some topology of connections. Examples include arrays of lasers [2], Josephson-junction arrays [3], neural networks [4], and chemical reactions [5]. The particular case of the dynamics of two coupled nonlinear oscillators is of interest since many fundamental dynamical scenarios can be investigated in considerable detail and can help guide and inform studies of more complex systems. In the case of weakly coupled oscillators, the phase is typically the most relevant variable to describe the dynamical response of the system since the amplitudes remain almost unchanged due to the weak interaction. However, for moderate to large coupling strengths, resonances and nonlinearities due to extra degrees of freedom assume an important role. In such situations the phase description is no longer sufficient and an investigation of the evolution must take amplitude effects into account. Even in the case of a single forced nonlinear oscillator many instabilities, homoclinic and heteroclinic phenomena, and complex dynamical behaviors arise.

Coupled semiconductor lasers are a good example of interacting nonlinear oscillators and are relevant for a number of applications. They can be used to provide either enhanced stability or highly irregular operation depending on the application. For example, they can be used for ultrashort pulse generation [6] where a very stable operation is highly desired to maximize the quality and repetition rate of the pulses generated. Conversely, they can be used in chaotic communication [7] where an irregular behavior is highly desired. With regard to coupled nonlinear oscillators as well as the potential for applications, understanding the nonlinear dynamics of coupled semiconductors lasers has been a topic of intense research. With the development of novel types of semiconductor devices, constant miniaturization, and promises of all optical integrated devices for large-scale photonic applications, the topic remains a very active area [8–12].

In this paper we examine theoretically the transition from master-slave to delayed mutual coupling for two single-mode semiconductor lasers coupled via their optical fields. Using a master-slave configuration as the starting point, we analyze how the coupled system changes when we allow part of the output of the slave laser to be injected into the master laser. We mostly consider a small physical separation between the lasers (the short delay regime) to make the analysis simpler but still sufficiently complicated to discuss some phenomena associated with the influence of the delay and the asymmetric mutual coupling in the system. In real-world applications a perfect symmetric coupling is rarely achieved and understanding the effect of this asymmetry is of practical interest. Also the coupling could be intentionally tuned to the asymmetric case depending on the application, once the effects are known. We describe the transition for both highly damped and weakly damped Class-B lasers [13]. Conventional quantum-well-based semiconductor lasers are well described by the usual Class-B equations, while in Ref. [14] it was shown that the steady-state behavior arising from saddle-node and Hopf bifurcations of optically injected quantum-dot lasers is qualitatively similar to that of optically injected Class-A lasers, providing further practical motivation for studying the strongly damped system. In addition, we briefly discuss the influence of the linewidth enhancement factor in the locking structure. The continuation packages AUTO [15] and DDEBIFTOOL [16] were used throughout the work.

II. PHASE-COUPLED OSCILLATORS

Although a very simple description, a phase model provides useful theoretical insights about the locking structure of a system, which could be applicable in some specific and practical situations such as for weakly coupled lasers with high relaxation oscillation damping. Weakly coupled quantum-dot lasers are excellent candidates for such a model [8,17] due to their strong relaxation oscillation damping characteristics. Further, phase models are of interest to researchers in diverse fields studying systems of coupled oscillators in a more general context [1,18,19]. In order to reveal some of the fundamentals of the phase-locking structure that are not influenced by

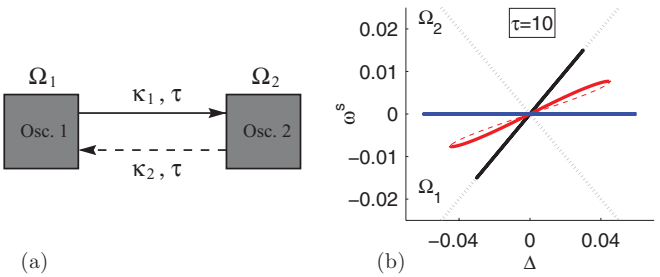

FIG. 1. (Color online) (a) Schematic of the two coupled oscillators with frequencies Ω_1 and Ω_2 and coupling strengths κ_1 and κ_2. (b) Phase-locked states for three representative situations: unidirectional coupling (black line following Ω_1), bidirectional with symmetric coupling (blue horizontal line), and bidirectional with asymmetric coupling (red line). Solid and dashed lines denote stable and unstable solutions, respectively. The frequency of the solutions is denoted by ω^s. Free-running frequencies Ω_1 and Ω_2 are illustrated by dotted lines.

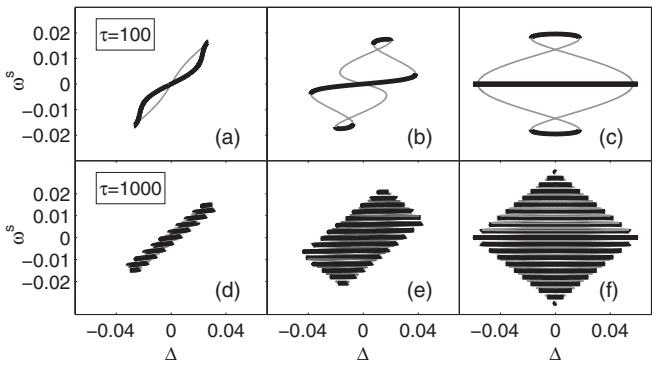

FIG. 2. Phase-locked states for the two mutually coupled oscillators. The frequency of the solutions is denoted by ω^s. Thick lines denote stable locking and thin lines denote unstable locking. The coupling strength $\kappa_1 = 0.03$ is fixed and the ratio of couplings κ_2/κ_1 is varied. Top: $\kappa_2/\kappa_1 = 0.1$ (a), 0.5 (b), and 1 (c) for $\tau = 100$. Bottom: $\kappa_2/\kappa_1 = 0.1$ (d), 0.5 (e), and 1 (f) for $\tau = 1000$.

amplitude variations or carrier effects, we perform an analysis of the delay-coupled phase model here. We are particularly concerned with phase-locked solutions. These are solutions where both oscillators have the same constant frequency and a fixed relative phase. In particular, we show that the phase model predicts a very regular structure for the phase-locked states in the mutually coupled configuration. The equations are

$$\begin{aligned}\dot{\phi}_1 &= \frac{\Delta}{2} - \kappa_2 \sin[\phi_1(t) - \phi_2(t-\tau)],\\ \dot{\phi}_2 &= -\frac{\Delta}{2} - \kappa_1 \sin[\phi_2(t) - \phi_1(t-\tau)].\end{aligned} \tag{1}$$

Here ϕ_i is the phase of oscillator i, $\Delta = \Omega_1 - \Omega_2$ is the frequency detuning, where Ω_i is the free-running frequency of oscillator i, κ_i describes the coupling strengths, and τ is the delay time between the oscillators. The equations are written in a reference frame centered on the average solitary frequency of the oscillators.

A schematic of the coupling configuration of the oscillators is shown in Fig. 1(a). When $\kappa_2 = 0$, the coupling is unidirectional and Eqs. (1) are reduced to Adler's equation [20]. In this case the delay time between the oscillators does not influence the long-term behavior and it is well known that the system can display only two types of long-term behavior: either a phase-locked state or an unlocked state where both oscillators oscillate with different frequencies. When $\kappa_2 \neq 0$, the oscillators are mutually coupled and each influences the dynamics of the other. Schuster and Wagner [21] investigated the behavior of Eqs. (1) for the case of symmetric coupling, where they found that multiple locked solutions appear when varying the coupling strength and/or the delay time. Figure 1(b) illustrates the locking range and the effect of changing the coupling from unidirectional to bidirectional. For the delay and coupling levels used in Fig. 1(b), only one stable locked solution and one unstable locked solution coexist, created by a saddle-node bifurcation. In the unidirectional limit, the stable and unstable frequencies are equal and both match the master frequency. The asymmetric coupling breaks this symmetry and the stable and unstable frequencies differ, as shown in Fig. 1(b). Increasing the coupling ratio, the locking frequency moves toward the center between the two free-running frequencies. In the symmetric bidirectional coupling limit, the stable and unstable frequencies are degenerate again and the locking frequency is centered between the free-running frequencies of the two oscillators.

Multiple solutions appear when the coupling strength κ_2 and the delay are increased. Figure 2 shows the locking frequency of the phase-locked solutions as a function of the detuning, computed for $\tau = 100$ and 1000 and for three different coupling ratios, where $\kappa_1 = 0.03$ is fixed. Figure 2(a) illustrates the situation where one coupling strength is very weak in comparison to the other and the system closely resembles the master-slave case with only one stable locked solution and one unstable locked solution. However, the branch of stable locked solutions is not a straight line anymore: Rather it is curved. For a certain level of the coupling strength κ_2, the branch of stable phase-locked solutions breaks, giving rise to multistable behavior. This phenomenon leads to the discretization of frequencies typically observed in delay-coupled systems [22,23]. The new coexisting phase-locked solutions appear through saddle-node bifurcations. The exact point where a single phase-locked solution bifurcates into two different phase-locked solutions is a cusp bifurcation, a codimension-2 point where two saddle-node curves meet. Figure 2(b) illustrates the case for a coupling ratio $\kappa_2/\kappa_1 = 0.5$ with three stable phase-locked solutions. (We will often refer to these phase-locked solutions simply as modes in this work.) Figure 2(c) shows the symmetric coupling case. The stable solutions are connected by unstable solutions. For larger delays the scenario described above is repeated and many coexisting modes can arise and multistable behavior appears for lower coupling ratios as the delay is increased. Figures 2(d)–2(f) show the case for $\tau = 1000$, illustrating the evolution of a very regular mode structure when the coupling strength κ_2 is increased up to the symmetric coupling case. For long delay times, the frequency difference between successive stable modes is approximately π/τ. Figure 3 shows magnifications of the mode structure and denotes typical solutions according to the phase difference $\psi = \phi_1 - \phi_2$ of the locked states.

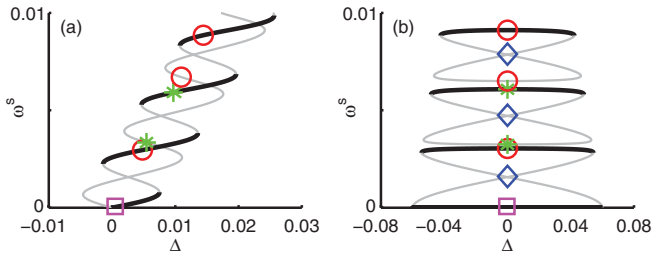

FIG. 3. (Color online) Magnification of Figs. 2(d) and 2(f) showing details of the branches of phase-locked solutions for (a) asymmetric coupling and (b) symmetric coupling. The frequency of the solutions is denoted by ω^s. Black lines denote stable solutions and gray lines denote unstable solutions. Asterisks (∗) indicate in-phase solutions, circles (○) indicate antiphase solutions, and squares (□) indicate where both coexist. Diamonds (◇) indicate out-of-phase solutions that exist for zero detuning in the symmetric coupling configuration.

The stable branches alternate between in-phase ($\psi = 0$) and antiphase ($\psi = \pi$) solutions. For the symmetric coupling case, out-of-phase solutions (solutions where $\psi \neq 0, \pi$) for zero detuning are also shown.

A useful diagram when investigating dynamics of coupled oscillators is the mapping of the synchronization region as a function of the detuning and coupling strength. For unidirectional coupling, the system is governed by Adler's equation and the locking region is the simplest possible, bounded by two straight lines formed by saddle-node bifurcations [Fig. 4(a)]. For bidirectional coupling, the two-parameter bifurcation structure of Eqs. (1), in the detuning-coupling space, is shown in Figs. 4(b)–4(d). Each diagram was computed for a fixed ratio

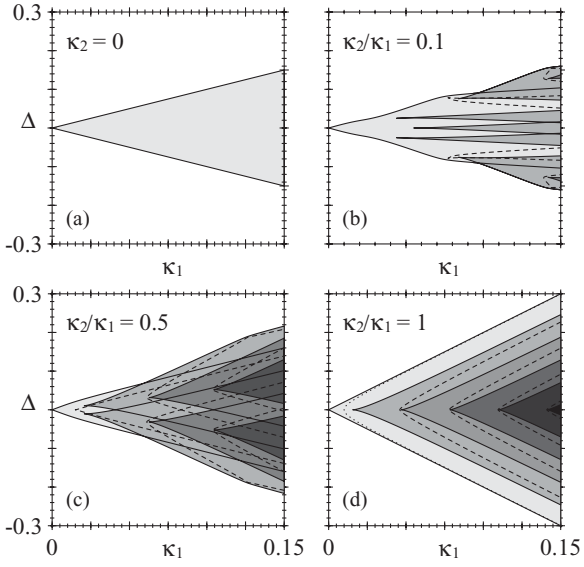

FIG. 4. Locking regions in the coupling-detuning space for Eqs. (1). Different gray tones denote different stable phase-locked solutions. Thick lines denote saddle-node bifurcations for stable solutions. Dotted and dashed lines denote pitchfork and saddle-node bifurcations, respectively, for unstable solutions. (a) Unidirectional coupling (the Adler case), (b) and (c) asymmetric bidirectional coupling, and (d) symmetric bidirectional coupling.

between the coupling strengths. When varying the coupling strength κ_1 in the horizontal axis, κ_2 is varied in such way that the ratio κ_2/κ_1 is constant. In this way it is possible to observe the effect of the asymmetric coupling for several levels of coupling strength as a function of the detuning between the two oscillators. Figure 4(b) shows the locking region for an asymmetric bidirectional coupling, where $\kappa_2/\kappa_1 = 0.1$. For low values of κ_1 only one stable mode exists. For higher κ_1 new modes are created through cusp bifurcations, leading to multiple coexisting phase-locked solutions for higher levels of coupling. Figure 4(c) shows the locking region for $\kappa_2/\kappa_1 = 0.5$. Here multistability appears for lower values of κ_1 since the coupling ratio is larger. Figure 4(d) shows symmetric bidirectional coupling. For small κ_1 just one mode exists. On increasing κ_1 a pitchfork bifurcation occurs and a pair of unstable modes is born. For higher levels of coupling and/or delay, additional modes are created in a structure of nested saddle-node V shapes.

III. DELAY-COUPLED SINGLE-MODE LASERS

A realistic description of a laser system has to take phase and amplitude into account. Amplitude effects become particularly important in the coupled laser system when the coupling is strong. The coupling strength at which instabilities first arise depends on many factors, in particular the relaxation oscillation damping, as we will discuss below. Here we consider two coupled single-mode semiconductor lasers modeled by standard rate equations for the electric fields and carrier densities. The model [24] is given by

$$\begin{aligned}
\dot{E}_1 &= (1 + i\alpha)N_1 E_1 + \kappa_2 e^{-i\Omega_0\tau} E_2(t-\tau) + \tfrac{1}{2} i\Delta E_1, \\
\dot{E}_2 &= (1 + i\alpha)N_2 E_2 + \kappa_1 e^{-i\Omega_0\tau} E_1(t-\tau) - \tfrac{1}{2} i\Delta E_2, \\
\dot{N}_1 &= \gamma[P - N_1 - (1 + 2N_1)|E_1|^2], \\
\dot{N}_2 &= \gamma[P - N_2 - (1 + 2N_2)|E_2|^2].
\end{aligned} \tag{2}$$

The equations are written in the reference frame of the average frequency of the free-running lasers. Here E_i and N_i are the complex electric field and the carrier density for laser i, respectively. The two lasers are identical except for their frequencies. The term α is the linewidth enhancement factor, P is the pump current above threshold, γ is the ratio of the photon lifetime and the carrier lifetime, τ is the coupling delay due to the finite-time propagation of the light, κ_i describes the coupling strengths, $\Omega_0 = \frac{\Omega_1 + \Omega_2}{2}$ is the average optical frequency where Ω_i is the free-running angular frequency of laser i, and $\Delta = \Omega_1 - \Omega_2$ is the frequency detuning. We assume that $\Omega_0\tau = 0 \bmod (2\pi)$, meaning that the spatial separation between the lasers is an integer number of the average optical wavelength. For studies of the effect of varying this parameter see Refs. [25,26], for example. The relaxation oscillations of the free-running lasers are characterized by γ and P. For P fixed, γ is proportional to the damping of the relaxation oscillations and we will refer to this important parameter somewhat loosely as the damping for the rest of this work. In this model, we define a phase-locked solution to be one where the two lasers oscillate at the same constant frequency with a fixed relative phase and with constant intensities and carrier densities, although the intensity and

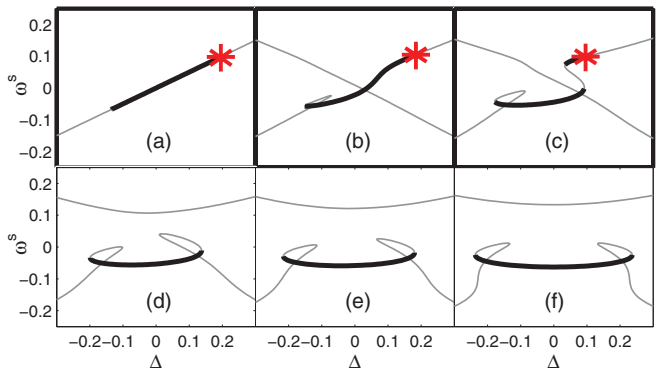

FIG. 5. (Color online) Frequency-locked states for different values of κ_2/κ_1 in the rate equation model [Eqs. (2)], from the unidirectional limit to the symmetric bidirectional limit. Black lines denote stable locking and gray lines denote unstable locking. Hopf bifurcations are denoted by asterisks (∗). The parameters $\alpha = 1.5$, $\tau = 10$, $\kappa_1 = 0.1$, $\gamma = 1$, and $P = 0.1$ throughout. The coupling ratio $\kappa_2/\kappa_1 = 0$ (master-slave) (a), 0.1 (b), 0.3 (c), 0.5 (d), 0.7 (e), and 1 (f).

carrier density of each device may be different from those of the other.

The master-slave system is described by Eqs. (2) with $\kappa_2 = 0$. In this case, laser 1 is referred to as the master and laser 2 as the slave. This system has been extensively studied and vast literature exists. See Ref. [27] for a review of the subject focusing on Class-B semiconductor lasers, Ref. [28] for Class-A lasers, and Ref. [14] for recent results on highly damped quantum-dot lasers. The effect of changing from unidirectional to symmetric bidirectional coupling for two representative values of γ is illustrated in Figs. 5 and 6, where the frequencies of the phase-locked solutions are plotted versus the detuning for different values of the coupling ratio κ_2/κ_1. The resulting frequencies are the same regardless of the value of γ. What is affected is the stability of these solutions as shown by comparing the corresponding figures: Certain ranges that are stable in Fig. 5 are unstable in Fig. 6. This is a typical effect of stronger damping, which enhances the stability properties of the system. Figures 5(a) and 6(a) show the master-slave unidirectional coupling states where the frequency of the slave laser just follows the frequency of the master. The transition to the stable locked regime is through

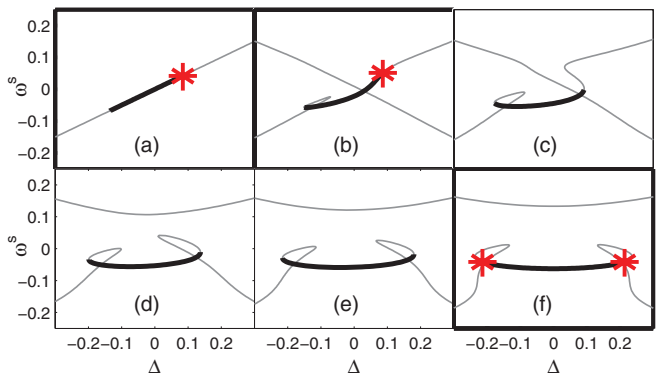

FIG. 6. (Color online) Same as Fig. 5, but for $\gamma = 0.005$.

a Hopf bifurcation for positive detuning and through a saddle node for negative detuning. When bidirectional coupling is introduced, many features shown in Sec. II for the phase model are seen again here, albeit with some extra complications such as the asymmetry introduced by the nonzero α factor. Figure 5(b) shows the case for a small coupling ratio and the branch of stable locked solutions has become curved. The frequencies of the stable and unstable solutions are no longer the same. For κ_2 above a certain level multistability arises for some range of the detuning, as shown in Fig. 5(c). Increasing the coupling κ_2 still further, a branch switching occurs [Figs. 5(d)–5(f)]. Such branch switchings are very common as the coupling strengths are increased individually or in tandem. One of the stable branches loses stability and only a single stable solution exists for this parameter configuration.

A better understanding of the scenarios discussed in the preceding paragraph is obtained by investigating the two-parameter evolution of the locking region as a function of the coupling ratio. Figure 7 shows numerically computed bifurcation diagrams for a short delay time $\tau = 10$. Figures 7(a)–7(f) represent the evolution from the unidirectional to the symmetric bidirectional coupling for a high damping and Figs. 7(g)–7(l) represent the evolution for weak damping. Let us consider the high damping case first.

Figure 7(a) shows the unidirectional master-slave stability diagram. Only the principal saddle-node and Hopf bifurcations are shown. (There are many other bifurcations even in the unidirectional system not considered in this work and many of these are explored in Ref. [27].) The shaded areas are those where there are stable phase-locked solutions. The diagram is asymmetric because of the nonzero α factor. Moving to Fig. 7(b), κ_2 is now nonzero but still small and the diagram is unchanged qualitatively. Thus, even with the introduction of the mutual coupling, the stability diagram can remain qualitatively similar to the unidirectional system. In Fig. 7(c) a second stable phase-locked solution has emerged coexisting with the first and so giving rise to multistability. This solution has arisen via a new saddle-node bifurcation induced by the delay in the system. As κ_2 is further increased the diagram becomes more and more symmetric while various new bifurcations appear. Finally, in Fig. 7(f) the coupling is symmetric and so the diagram also becomes symmetric. A third stable phase-locked solution has also appeared. The similarity to the phase model at low levels of κ_1 is clear. The nested-V structure is evident and if one increased the delay this would be even more evident as the high delay would result in many more stable phase-locked solutions. This similarity to the phase model is expected. The higher the damping, the less important carrier effects become and so for high damping the system depends predominantly on the electric field while in the class-A limit $\gamma \gg 1$ the carrier effects can be adiabatically eliminated. For low coupling strengths the electric-field amplitude is less important and so one would expect good agreement with the phase model [17].

Figures 7(g)–7(l) show the corresponding stability diagrams for weakly damped devices. Figure 7(g) shows the unidirectional diagram. As κ_2 is increased various new bifurcations arise. Of particular interest are the white regions within the principal saddle-node V shape evident in Figs. 7(j)–7(l). In these regions there are no stable phase-locked solutions.

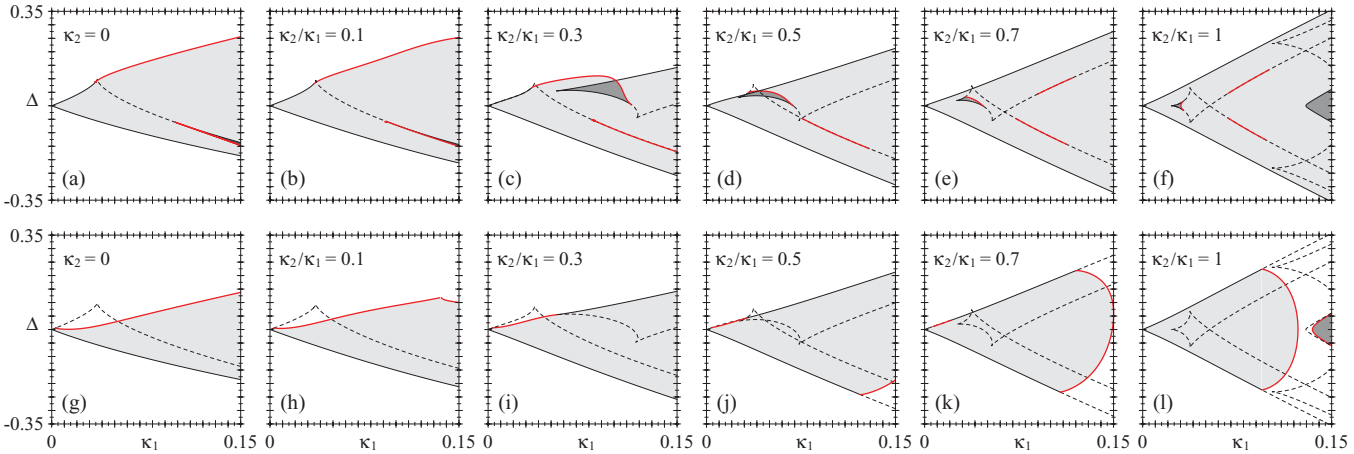

FIG. 7. (Color online) Evolution of the locking region when increasing the coupling ratio κ_2/κ_1 from unidirectional to the symmetric bidirectional case, for a short delay time between the lasers ($\tau = 10$). The upper row shows the case for strong damping ($\gamma = 1$) and the bottom row shows that for weak damping ($\gamma = 0.005$). Black (red) lines denote saddle-node (Hopf) bifurcations and solid (dashed) lines refer to stable (unstable) locked states. Only stable Hopf bifurcations are shown. The parameters $P = 0.1$ and $\alpha = 1.5$ throughout. Different gray tones denote different stable phase-locked solutions.

A second stable phase-locked solution has appeared in Fig. 7(l), again induced by the delay in the system. It is instructive to compare and contrast the two rows. The main differences are the enhanced stability and the extra solutions both found for high γ. The locking region is larger and there are more phase-locked solutions in general for the highly damped system. We see that there is at least one stable phase-locked solution at every coupling strength for the highly damped lasers in contrast to the weakly damped lasers. In fact, with weak damping there are coupling strengths at which stable phase locking is not even possible at zero detuning. This instability is a result of both a nonzero α and the low damping and occurs through a Hopf bifurcation. One would expect the resulting limit cycle to combine both relaxation oscillation and coupling characteristics. An analytic investigation of the frequency of this cycle would be interesting. Similar absences of stable phase locking have also been reported in Refs. [11,12] where in both cases weakly damped lasers were investigated. Highly damped quantum dot lasers, in contrast, have demonstrated stable phase-locking properties when mutually coupled at all tested coupling strengths and even for long delay times [8,17].

Clearly the diagrams display a combination of unidirectional coupling effects and feedbacklike-delay-induced effects. As κ_2 is increased the master-slave locking boundaries are deformed continuously and even in the fully symmetric bidirectional coupling limit the external saddle-node boundary is a remnant of the original master-slave line. The emergence of new saddle-node bifurcations is preserved from the phase model and is a delay-induced feature also found in systems with delayed feedback. The emergence of the Hopf bifurcations through amplitude effects provides the principal difference with the phase model.

Optically injected weakly damped lasers undergo a stable Hopf bifurcation even for very low injection levels causing self-sustained oscillations at the relaxation oscillation frequency. However, stable Hopf bifurcations do not arise for highly damped and class-A lasers at weak injection levels. In Fig. 7 we show only the stable Hopf bifurcations, but of course it is also possible to find the unstable Hopf bifurcations. Figure 8 shows the symmetric bidirectional coupling diagrams with both stable and unstable Hopf bifurcations. The weakly damped case is much more complicated than the strongly damped case, as one might expect. From an experimental point of view, these curves are not very important since they do not give rise to stable solutions. Interestingly, the Hopf bifurcations at very low coupling strengths in the weakly damped system are all unstable and the saddle node provides the locking boundary while there is a stable Hopf bifurcation in the highly damped case conferring stability on a second phase-locked solution, demonstrating that the Hopf bifurcations are not always instability inducing.

Increasing the delay time greatly complicates the two-parameter locking diagrams of Fig. 7. Instead, we plot the frequency of the phase-locked solutions versus the detuning in Fig. 9. In Fig. 9 we consider a delay time of $\tau = 100$, ten times that used for Fig. 7. This induces many extra phase-locked solutions (both stable and unstable) and, in particular, multistability exists for both the weakly damped and strongly damped systems. As before, the number of stable

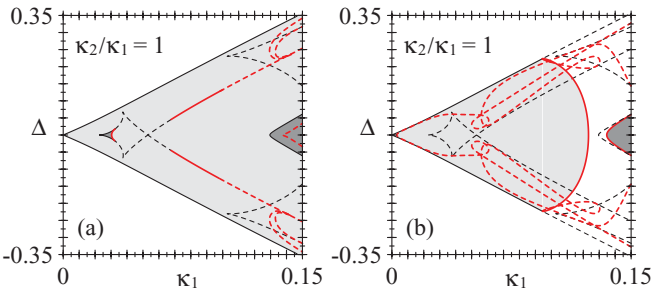

FIG. 8. (Color online) Symmetric bidirectional stability diagrams. (a) Same as in Fig. 7(f), but with the unstable Hopf bifurcations also shown. (b) Same as in Fig. 7(l), but with the unstable Hopf bifurcations also shown. Different gray tones denote different stable phase-locked solutions.

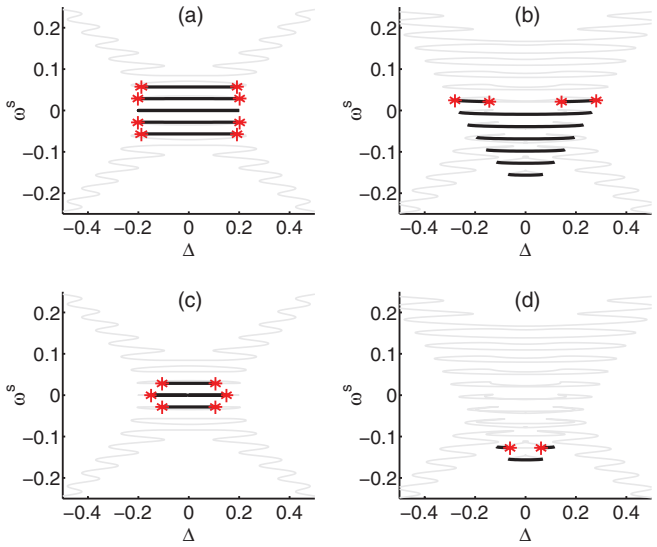

FIG. 9. (Color online) Mode structure for symmetric coupling for strongly damped and weakly damped systems. Here $\kappa_1 = \kappa_2 = 0.1$, $\tau = 100$, and $P = 0.1$. Top: $\gamma = 1$ and (a) $\alpha = 0$ and (b) $\alpha = 1.5$. Bottom: $\gamma = 0.005$ and (c) $\alpha = 0$ and (d) $\alpha = 1.5$. Black (gray) lines denote stable (unstable) solutions and asterisks (∗) denote Hopf bifurcations.

solutions is larger for the case of strong damping. Figure 9 also illustrates some effects of the α factor on the locking structure. As already mentioned, the unidirectional stability diagram is asymmetric for $\alpha \neq 0$ and this asymmetry is maintained for the bidirectional coupling system except in the symmetric bidirectional limit. However, an asymmetry due to the α factor is still observed in the set of phase-locked solutions even for symmetric bidirectional coupling. In this case, the asymmetry is to be found in the frequency of the locked solutions and so in the (vertical) ω^s axis in Fig. 9. For $\alpha = 0$ the frequency solutions are centered on the average free-running frequency and the figure is symmetric both in the detuning and in ω^s. However, for nonzero α this is no longer true and while it is symmetric in the detuning it is asymmetric in ω^s.

IV. CONCLUSION

We discussed the transition from master-slave to delayed mutual coupling of two semiconductor lasers by tuning the coupling strengths between the two limits. First we analyzed a simple model described by the phase of the lasers only. This has a broad relevance since many coupled oscillator models can be reduced to phase models when the coupling is sufficiently weak. In particular, we described the creation of several stable phase-locked solutions formed in a series of codimension-2 cusp bifurcations as the coupling strength is increased. We then considered the standard coupled rate equation model for semiconductor lasers for two representative values of the relaxation oscillation damping, one strong and one weak. The locking behavior combines effects from the unidirectional coupling and the optical feedback configurations. We showed how the locking region changes due to the influence of the mutual coupling and that several features of the master-slave system remain in the mutually coupled system. It was shown that the stability of the phase-locked states is very different when comparing the situations of strong and weak damping as one would naturally expect; the strong damping enhances the stability properties of the system. This can be seen in terms of larger locking ranges and more stable phase-locked states. It would be interesting to examine the evolution of the region where no stable phase locking can occur for any detuning with changing delay and γ and this may form the basis of future work.

A further challenge now is to develop similar transition scenarios for dynamics including more complex regimes such as pulsating and chaotic solutions and noise-induced phenomena such as excitability [27,29] that are well known to occur in the master-slave system. As shown in Fig. 7, even with the introduction of appreciable mutual coupling, the stability diagram can remain qualitatively identical to the master-slave diagram and so one should expect certain dynamical features of the master-slave system to persist while the influence of the delay may provide some different features. Such an effect has been considered in the case of symmetric bidirectional coupling and excitable pulsations in Ref. [17], where pulse trains rather than excitable pulses were found.

ACKNOWLEDGMENTS

B.K. thanks David Goulding for discussions. This research was enabled by the Higher Education Authority Program for Research in Third Level Institutions (2007–2011) via the INSPIRE program and the authors also gratefully acknowledge the support of Science Foundation Ireland under Contract No. 07/IN.1/I929.

[1] Y. Kuramoto, *Chemical Oscillations, Waves, and Turbulence* (Springer, Berlin, 1984); A. Pikovsky, M. Rosenblum, and J. Kurths, *Synchronization: A Universal Concept in Nonlinear Sciences* (Cambridge University Press, Cambridge, 2003); S. H. Strogatz, *Sync: The Emerging Science of Spontaneous Order* (Penguin Science, New York, 2004).

[2] *Diode Laser Arrays*, edited by D. Botez and D. R. Scifres (Cambridge University Press, Cambridge, 1994).

[3] K. Wiesenfeld, P. Colet, and S. H. Strogatz, Phys. Rev. Lett. **76**, 404 (1996).

[4] W. Gerstner and W. M. Kistler, *Spiking Neuron Models Single Neurons, Populations, Plasticity* (Cambridge University Press, Cambridge, 2002).

[5] I. Z. Kiss, Y. M. Zhai, and J. L. Hudson, Science **296**, 1676 (2002).

[6] P. Vasilev, *Ultrafast Diode Lasers: Fundamentals and Applications* (Artech House, Boston, 1995).

[7] G. D. VanWiggeren and R. Roy, Science **279**, 1198 (1998); A. Argyris, D. Syvridis, L. Larger, V. Annovazzi-Lodi, P. Colet, I. Fischer, J. Garcia-Ojalvo, C. R. Mirasso, L. Pesquera, and K. A. Shore, Nature (London) **438**, 343 (2005).

[8] S. P. Hegarty, D. Goulding, B. Kelleher, G. Huyet, M.-T. Todaro, A. Salhi, A. Passaseo, and M. De Vittorio, Opt. Lett. **32**, 3245 (2007).

[9] N. Rebrova, T. Habruseva, G. Huyet, and S. P. Hegarty, Appl. Phys. Lett. **97**, 101105 (2010).

[10] P. Heinricht, B. Wetzel, S. O'Brien, A. Amann, and S. Osborne, Appl. Phys. Lett. **99**, 011104 (2011).
[11] S. Wieczorek and W. W. Chow, Opt. Commun. **246**, 471 (2005); H. Erzgräber, S. Wieczorek, and B. Krauskopf, Phys. Rev. E **81**, 056201 (2010).
[12] H. Erzgräber, E. Wille, B. Krauskopf, and I. Fischer, Nonlinearity **22**, 585 (2009).
[13] F. T. Arecchi, G. L. Lippi, G. P. Puccioni, and J. R. Tredicce, Opt. Commun. **51**, 308 (1984).
[14] T. Erneux, E. A. Viktorov, B. Kelleher, D. Goulding, S. P. Hegarty, and G. Huyet, Opt. Lett. **35**, 937 (2010).
[15] E. J. Doedel, R. Paffenroth, A. R. Champneys, T. F. Fairgrieve, Y. A. Kuznetsov, B. E. Oldeman, B. Sandstede, and X. Wang, AUTO2000: Continuation and Bifurcation Software for Ordinary Differential Equations (with HomCont), 2000, [http://www.sourceforge.net/projects/auto2000/].
[16] K. Engelborghs, T. Luzyanina, and G. Samaey, DDE-BIFTOOL v. 2.00 User Manual: A MATLAB Package for Bifurcation Analysis of Delay Differential Equations, Report TW-330, Department of Computer Science, Katholieke Universiteit Leuven, Belgium, 2001.
[17] B. Kelleher, C. Bonatto, P. Skoda, S. P. Hegarty, and G. Huyet, Phys. Rev. E **81**, 036204 (2010).
[18] M. K. Stephen Yeung and S. H. Strogatz, Phys. Rev. Lett. **82**, 648 (1999).
[19] O. D'Huys, R. Vicente, T. Erneux, J. Danckaert, and I. Fischer, Chaos **18**, 037116 (2008).
[20] R. Adler, Proc. IRE **34**, 351 (1946) [reprinted in Proc. IEEE **61**, 1380 (1973)].
[21] H. G. Schuster and P. Wagner, Prog. Theor. Phys. **81**, 939 (1989).
[22] H.-J. Wünsche, S. Bauer, J. Kreissl, O. Ushakov, N. Korneyev, F. Henneberger, E. Wille, H. Erzgräber, M. Peil, W. Elsäßer, and I. Fischer, Phys. Rev. Lett. **94**, 163901 (2005).
[23] S. Yanchuk, Phys. Rev. E **72**, 036205 (2005).
[24] J. Mulet, C. Masoller, and C. R. Mirasso, Phys. Rev. A **65**, 063815 (2002).
[25] S. Yanchuk, K. R. Schneider, and L. Recke, Phys. Rev. E **69**, 056221 (2004).
[26] H. Erzgräber, D. Lenstra, B. Krauskopf, E. Wille, M. Peil, I. Fischer, and W. Elsäßer, Opt. Commun. **255**, 286 (2005).
[27] S. Wieczorek, B. Krauskopf, T. B. Simpson, and D. Lenstra, Phys. Rep. **416**, 1 (2005).
[28] C. Mayol, R. Toral, C. R. Mirasso, and M. A. Natiello, Phys. Rev. A **66**, 013808 (2002).
[29] D. Goulding, S. P. Hegarty, O. Rasskazov, S. Melnik, M. Hartnett, G. Greene, J. G. McInerney, D. Rachinskii, and G. Huyet, Phys. Rev. Lett. **98**, 153903 (2007); B. Kelleher, D. Goulding, S. P. Hegarty, G. Huyet, Ding-Yi Cong, A. Martinez, A. Lemaître, A. Ramdane, M. Fischer, F. Gerschütz, and J. Koeth, Opt. Lett. **34**, 440 (2009); B. Kelleher, C. Bonatto, G. Huyet, and S. P. Hegarty, Phys. Rev. E **83**, 026207 (2011).